



**HAL**  
open science

## Monitoring and modeling the deposition of metal nanoparticles on surfaces by impedance

Rafael C Hensel, Maria H Gonçalves, Kevin L Rodrigues, Vitor T.A. Oiko, Vinicius Do L. Pimentel, Marcelo A Pereira-Da-Silva, Matthias Hillenkamp, Antonio Riul Jr., Varlei Rodrigues

► **To cite this version:**

Rafael C Hensel, Maria H Gonçalves, Kevin L Rodrigues, Vitor T.A. Oiko, Vinicius Do L. Pimentel, et al.. Monitoring and modeling the deposition of metal nanoparticles on surfaces by impedance. Applied Surface Science, 2021, 544, pp.148806. 10.1016/j.apsusc.2020.148806 . hal-03113031

**HAL Id: hal-03113031**

**<https://hal.science/hal-03113031>**

Submitted on 18 Oct 2021

**HAL** is a multi-disciplinary open access archive for the deposit and dissemination of scientific research documents, whether they are published or not. The documents may come from teaching and research institutions in France or abroad, or from public or private research centers.

L'archive ouverte pluridisciplinaire **HAL**, est destinée au dépôt et à la diffusion de documents scientifiques de niveau recherche, publiés ou non, émanant des établissements d'enseignement et de recherche français ou étrangers, des laboratoires publics ou privés.

# Monitoring and modeling the deposition of metal nanoparticles on surfaces by impedance

Rafael C. Hensel<sup>a</sup>, Maria H. Gonçalves<sup>a</sup>, Kevin L. Rodrigues<sup>a,b</sup>, Vitor T. A. Oiko<sup>a,c</sup>, Vinicius do L. Pimentel<sup>d,e</sup>, Marcelo A. Pereira-da-Silva<sup>f,g</sup>, Matthias Hillenkamp<sup>a,h</sup>, Antonio Riul Jr.<sup>a</sup>, Varlei Rodrigues<sup>a,\*</sup>

<sup>a</sup>*Instituto de Física "Gleb Wataghin", Universidade Estadual de Campinas, 777 Sérgio Buarque de Holanda Street - Cidade Universitária Zeferino Vaz, Campinas - SP, Brazil.*

<sup>b</sup>*Departamento de Física Instituto de Ciências Exatas, Universidade Federal de Minas Gerais, 6627 Av. Pres. Antônio Carlos, Belo Horizonte - MG, Brazil.*

<sup>c</sup>*The University of Manchester, Oxford Road, Manchester, M13 9PL, United Kingdom.*

<sup>d</sup>*Centro de Tecnologia da Informação Renato Archer, Rodovia Dom Pedro I (SP-65), Km 143,6, Campinas - SP, Brazil.*

<sup>e</sup>*Faculdade de Engenharia Elétrica e de Computação, Universidade Estadual de Campinas, 400 Albert Einstein Avenue - Cidade Universitária Zeferino Vaz, Campinas - SP, Brazil.*

<sup>f</sup>*Instituto de Física de São Carlos - IFSC/USP, São Carlos - SP, Brazil.*

<sup>g</sup>*Centro Universitário Central Paulista - UNICEP, São Carlos - SP, Brazil.*

<sup>h</sup>*Institute of Light and Matter, University of Lyon, University Claude Bernard Lyon 1, CNRS, UMR5306, F-69622 Villeurbanne, France.*

---

## Abstract

The study of metallic nanoparticles (NPs) on surfaces and their properties has become a common subject for a variety of areas. Notably, to exploit the unique intrinsic features of deposited NPs in macroscopic devices, samples with low coverage are required. The electrical characterization techniques has, however, so far been limited mostly to systems near or beyond the percolation limit, when the nanostructure's resistive behavior is dominant. Here we describe the impedance response of interdigitated electrodes (IDE) during Ag NP deposition, from the very beginning up to the percolation limit. Our experiments present two regimes: up to  $\sim 20\%$  of coverage the capacitance grows linearly with the deposition, increasing abruptly afterward. To understand the experimental data, we propose a model in which the capacitance response is attributed to isolated and agglomerated NPs. Initially, isolated NPs contribute to the ca-

---

\*Corresponding author

Email address: [varlei@ifi.unicamp.br](mailto:varlei@ifi.unicamp.br) (Varlei Rodrigues)

capacitive response. Beyond  $\sim 20\%$  coverage, shielded regions of the IDE due to agglomerated NP islands start to dominate until eventually percolation leads to a predominantly conductive signal. These interpretations are supported by Electron Microscopy and Atomic Force Microscopy. The proposed analysis allows improving the control of the concentration of NP deposited on surfaces systems with low coverage by impedance monitoring.

*Keywords:* magnetron sputter nanoparticle deposition, mass selected nanoparticle, nanoparticle thin films, in-situ impedance measurement, silver, capacitance behavior modeling

---

## 1. Introduction

Nanostructuring paved the way to a plethora of exciting possibilities, from fundamental studies to new applications. These systems can present properties that differ sharply from their macroscopic scale counterpart or even show  
5 new and unexpected effects. Metallic nanoparticles (NP) and thin films, both examples of systems widely studied in this context, show optical [1, 2, 3], electrical [4] and catalytic [5] properties with great potential for new technological applications. Significant advances have been achieved in studying the electrical properties of metallic NP films. [6, 7] Most of these studies are based on samples  
10 fabricated by atom deposition. [8, 9] However, in this process, the nanostructure growth depends on the diffusion of metal atoms on the surface of the substrate. [10] In this context, the control, and modeling of the electrical properties of metallic NP thin films is crucial for the development and miniaturization of electronic devices and flexible electronics.

15 Electrical properties of metal films on surfaces obtained by the deposition of atoms are very complex because of the complicated interplay of different parameters like atom and island mobility on the surface, wettability and others [8, 9, 11, 12, 13]. Furthermore, films with metallic NPs as building blocks also present nanoscale and disorder effects that modify the electrical properties  
20 [14, 15]. J. E. Barborini *et al.* deposited Fe, Pd, Nb, W, and Mo clusters between

interdigitated electrodes (IDEs), planar devices composed of metallic digits on an insulating substrate, and performed DC electrical measurements during the film formation. By correlating the device resistivity evolution with the conduction path they show that the resistivity decreases by two orders of magnitude due to the transition from 1D to 2D conductive paths. The resistivity reaches a minimum, and then increases due to the formation of 3D conductive paths in nanostructured metal films [14]. A. Sattar *et al.* describe how tunnelling results in clearly non-classical conductance and how this quantum conductance can lead to switching behavior in percolating nanoparticle films [15]. O. Kylián *et al.* report that the resistivity of Pt nanoclusters film on Si and glass decreases three orders of magnitude while the film thickness increases up to 50 nm [10]. Recently, there were several reports on cluster assembled nanostructures that present memristive behavior. C. Minnai *et al.* reported switching behavior in Au cluster-assembled nanostructured films on glass substrates, which is attributed to the formation/destruction of conductive paths between particles [16]. M. Mirigliano *et al.* have reported the resistance evolution as a function of Au NP film thickness beyond the percolation limit and applied percolation theory to evaluate how the variation of nanoaggregates connectivity influence the memristive effect [17]. Recently, A. Vahl *et al.* applied conducting atomic force microscopy to investigate *in situ* individual alloy NP memristive effects and their structural degradation [18].

The vast majority of studies on electrical properties of NP films are based on DC measurements [14, 15, 19, 20, 21], that consider coverage at or above percolation, where electrical transport, by conduction or tunneling is possible. Our experiment addresses the regime well below percolation, where the individual NP properties are not or only slightly perturbed. Indeed, many studies on metallic NPs deposited on a surface, exploring magnetic [22, 23], optical [3], and catalytic [24] properties, are carried out in a low concentration regime, where the interactions between NPs are kept negligible in order to preserve the intrinsic nanoscale properties of the NPs [25, 26, 27]. In this article, we report an experimental method for *in situ* monitoring of Ag NP deposition between

the fingers of the IDEs via impedance measurement. This technique allows the IDE electrical characterization from the very start of deposition up to the percolation threshold. To understand the experimental data, we propose a model based on how randomly distributed metallic NPs affect the electric field between the IDE digits, which can also be translated as variations in the capacitance. The methodology proposed here allows for better control and interpretation of metallic NP deposition on surfaces. Our approach is versatile and can be applied to various nanostructured systems with NP deposition on surfaces or their integration into matrices, such as e.g. polymers [28]. The incorporation of metallic NP into a polymer system has, amongst many others, been exploited to tune sensor sensitivity and selectivity [29, 30, 31, 32] or to suppress lithium dendrite growth in lithium metal batteries [33]. Nevertheless, so far, NP deposition onto or into polymers has so far only been achieved leaving crucial parameters like the NP concentration out of reach. In this sense, the electrical monitoring of NP deposition is essential to define their concentration, which is typically chosen well below the percolation limit in order to better define the useful features of these devices.

## 2. Materials and Methods

### 2.1. *In situ impedance monitoring of IDE during NP deposition*

We fabricated NP using a gas aggregation source [34]. In this system, the erosion of a metal wire target produces a cloud of atoms. Collisions between sputtered atoms and cold Ar atoms promote NP formation. Figure 1(a) shows a scheme of the experimental setup used for the NP fabrication. A set of electrostatic lenses guides and focuses the positively charged NP beam onto the sample holder [35]. The set of lenses includes a Bessel box, allowing the selection of the NP mean size to be deposited on the sample holder. A small fraction of the NPs is deflected to a time-of-flight mass spectrometer (TOF) that keeps track of the NP size distribution during the whole experiment. The NP mean diameter was monitored throughout the whole experiment and was typically fixed to

$\sim 3$  nm. The major part of the NP beam is deposited on the sample holder or on a current detector with  $75 \text{ mm}^2$  area that monitors the charged NP deposition rate. To estimate the area covered by NPs, we consider the spherical NP projection in circles of area  $A_{NP}$ . We estimate the NP covered area according to 85  $\frac{A_{NP}}{A_{SENSOR}} \frac{t \times I}{e}$ , in which  $\frac{A_{NP}}{A_{SENSOR}}$  is the ratio between the NPs area and the current sensor area,  $t$  is the deposition time,  $e$  is the electron's charge and  $I$  is the NPs deposition current. The produced NP deposition current was monitored using a Keithley Series 6487 Picoammeter, with typical values of  $I = 330 \text{ pA}$ , corresponding to  $\sim 1.4 \times 10^{-4}$  monolayers/second

90 To investigate the Ag NP film electrical properties, we have deposited the produced NPs onto IDEs. Here, we used gold IDEs on glass, comprising 30 pairs of digits with 3 mm length, 200 nm height,  $40 \mu\text{m}$  width, and spaced  $40 \mu\text{m}$  from each other, fabricated at the Microfabrication Laboratory, National Center for Research in Energy and Materials, Brazil. We performed impedance 95 measurements to analyze *in situ* the evolution of the electrical properties of IDEs during Ag NP deposition, as schematically shown in Figure 1(b). Measuring *in situ* avoids NP oxidation, which is an important issue when using such small NPs [36]. The produced NPs are randomly deposited on the whole IDE but the NPs deposited on the IDE digits do not modify the overall electrical 100 properties. However, the NPs deposited between adjacent digits, equivalent to half of the total IDE area, do modify the electrical response, as illustrated in Figure 1(c). We perform impedance measurements using a homemade setup, described in detail elsewhere [37]. Briefly, a sinusoidal voltage of 1 V amplitude at 1 kHz is applied to one comb of digits of the IDE [37]. The current from 105 the pick-up electrode is amplified using an operational amplifier in a differential configuration. A lock-in system measures the output voltage and the phase shift between input and output signals in 0.5 s intervals. We interpret the complex impedance measurements using an equivalent circuit composed of a parallel coupling of capacitive and conductive components [37], which provides  $C = \frac{1}{\omega} \frac{\text{Im}(Z)}{|Z|^2}$  and  $G = \frac{\text{Re}(Z)}{|Z|^2}$ , respectively. The metal NP deposition between the IDE dig- 110 its modifies the device geometry. Considering that the region between adjacent

digits can be approximated by a parallel coupling of capacitors, the nanoparticle deposition decreases the gap of the capacitors, which is equivalent to having an series coupling of capacitors, as shown in Figure 1 (d). Consequently, the total

115 capacitance increases at the beginning of deposition.

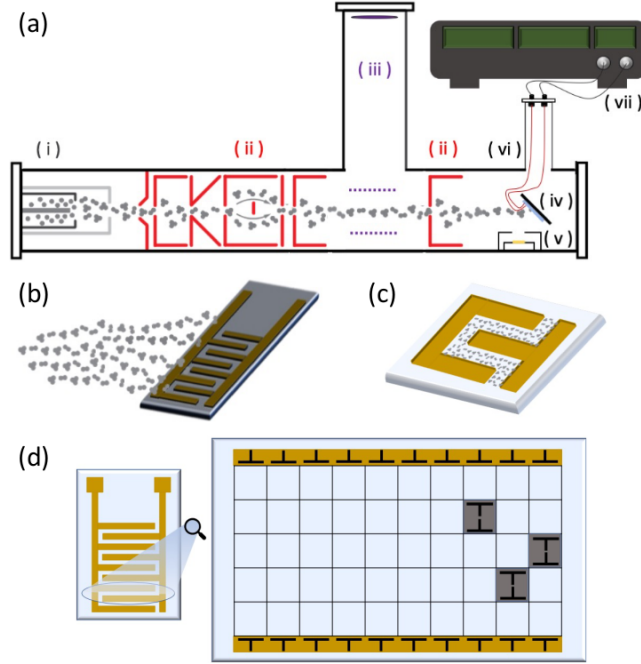


Figure 1: (a) Experimental setup scheme of the atomic cluster source connected to a complex impedance meter system. (i) Aggregation chamber where atoms are sputtered from a wire target and start aggregating in a low-temperature Ar atmosphere; (ii) electrostatic optics that guide, mass select and focus the NPs; (iii) time-of-flight mass spectrometer (TOF) for *in-situ* analysis of produced NP size; (iv) 45 ° sample holder where IDE is mounted for *in-situ* complex impedance monitoring; (v) neutralization filament to avoid charging effects on the sample; (vi) deposition chamber; (vii) complex impedance meter setup. (b) Sample holder details to illustrate the NP deposition on the IDE. Note that the IDE is rotated with respect to the sample holder position to better represent the deposition. (c) Although the NPs are deposited everywhere on the IDE, for clarity we show only the NPs deposited between adjacent digits. (d) Sketch to illustrate the region between adjacent digits of the IDE to show the parallel coupling of capacitors, and the capacitors in series after some sites (grey squares) are filled with nanoparticles.

## 2.2. *Ex situ morphology investigation*

We investigated the coverage and the topography of the NP film deposited on the IDE to interpret the electrical behavior observed. After the NP deposition, we analyzed the topography of the region between the IDE's digits using Atomic Force Microscopy (AFM), in a BRUKER Dimension ICON instrument, using a rectangular shaped silicon tip,  $42 \text{ Nm}^{-1}$  spring constant and 330 kHz free oscillation in tapping mode. Complementary information about the NP size evolution is obtained from Transmission Electron Microscopy (TEM) experiments. The NP size distribution and covered area on a surface were investigated on samples produced by the deposition of Ag NP for different deposition times on Ultrathin Carbon Film Supported by a Lacey Carbon Film on 400 Mesh Copper TEM grids. These grids were analyzed using a Jeol 2100F field emission gun TEM at the Electron Microscopy Laboratory, National Center for Research in Energy and Materials, Brazil.

## 3. Results

### 3.1. *Impedance monitoring of silver nanoparticle deposition*

Both the capacitance and conductance evolution, as a function of the fraction of area covered by the NPs, from the very beginning up to 50% coverage, is shown in Figure 2. At the beginning of the deposition, the measured capacitance value was  $C_{\text{IDE}} = 10.25 \text{ pF}$ , corresponding to the bare IDE in vacuum [38, 39]. A monotonic increase of capacitance following the NP coverage is observed even during the early stages of the deposition, demonstrating higher sensitivity as compared to conductivity DC measurements [14, 9]. Besides, Figure 2 allows us to infer that the capacitance measurements presents two growth regimes: an initial linear growth for the first 20% of the covered area, which becomes super-linear after 20% of covered area. The conductance measurements present no variation until  $\sim 20\%$ , followed by a steep increase. The measurement was stopped after one hour of deposition, which was equivalent to 50% of the estimated covered area.

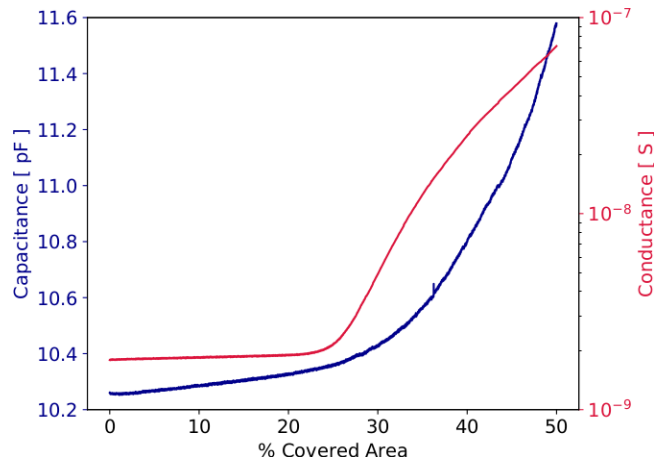


Figure 2: IDE capacitance (left-hand side y-axis), and conductance (right-hand side y-axis) variation as a function of the covered area during the deposition of 3 nm silver NPs.

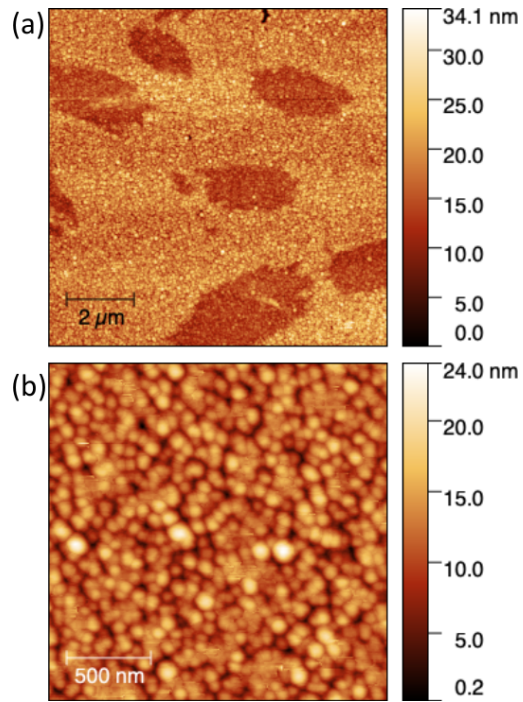


Figure 3: (a)  $10 \mu\text{m} \times 10 \mu\text{m}$  and (b)  $2 \mu\text{m} \times 2 \mu\text{m}$  AFM micrograph between IDE digits after the NP deposition. Note that the holes are related to incompletely filled NP layers.

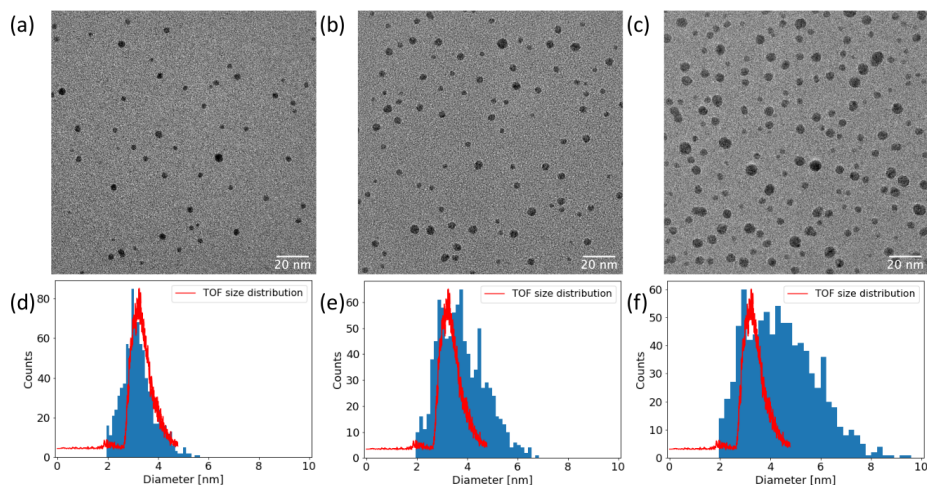


Figure 4: TEM micrographs of Ag NPs: (a) 1.5% covered area, (b) 5% covered area, (c) 11% covered area. We can observe that the NPs coalesced on the grid and increased their diameter with the covered area. Size distribution for (d) 1.5% , (e) 5% and (f) 11% covered area. The red curve is the time-of-flight size distribution during the sample preparation, which presents 3.2 nm for the NPs mean diameter.

145 *3.2. Morphological investigation of silver nanoparticle on surfaces*

To analyze the topography between adjacent digits, we performed an AFM analysis. Figure 3 shows an AFM micrograph of the IDE used to obtain the electrical behavior shown in Figure 2. As shown in Figure 3(a), the deposited NPs form an almost continuous thin film, with some incompletely filled islands. The mean height measurement in the depression regions is  $(4.0 \pm 0.5)$  nm, which is consistent with the NP diameter. Figure 3(b) was obtained where the NPs form a seemingly continuous film. We can observe that the NPs do not form an ordered packed film as assumed for the covered area estimation, but they are randomly distributed on the surface. The micrograph also shows that the NPs start to agglomerate on top of the unfilled layer of previously deposited NPs.

155 Figures 4(a-c) present TEM micrographs of Ag NPs for 1.5%, 5%, and 11% covered area, respectively. We observe that an increasing percentage of the covered area also increases the NP diameter due to aggregation. The size distribution obtained for these micrographs are compared with the time-of-flight size

160 distribution, shown in graphs 4(d-f). We can see that for 1.5% covered area,  
the NP size distribution derived from the TEM analysis coincides with the TOF  
size distribution obtained during deposition, reinforcing our monitoring method  
(Figure 4 (d)). Increasing the percentage of covered area shifts the NPs mean  
size and broadens the distribution towards bigger NPs, as shown in Figures 4(e)  
165 and (f), as already reported by H. Wei and H. Eilers [4].

## 4. Model

### 4.1. Capacitance evolution during silver nanoparticle deposition

The impedance monitoring during the 3 nm Ag NP deposition on a bare IDE  
shows a capacitance growth profile with the covered area, figure 2. In contrast  
170 to DC measurements, the capacitance measurements starts to increase from  
the very beginning of the deposition, which corresponds to the contribution  
of isolated NPs to the device capacitance. The variation in capacitance due  
to the NPs occurs because of the change in the electric field they cause when  
deposited in the area between digits. The IDE capacitance can be represented  
175 by an equivalent circuit of parallel capacitors that describe the contribution  
from different parts of the IDE to the total capacitance. For example, one  
capacitor can take into account the contribution from the top of the digits,  
and another the region between digits, where the field is parallel to the IDE  
substrate. Different parallel capacitors then describe this last region. In this  
180 sense, deposited NPs only affect one of these capacitors, representing a fraction  
of the capacitance due to the region between digits and close to the substrate  
surface. All other contributions remain constant during the experiment. In  
this sense we can write the total capacitance as a function of the covered area  
 $A$  by  $C_{\text{total}}(A) = C(A) + C'_0$  where  $C(A)$  was the capacitance due to the NP  
185 deposition and  $C'_0$  the part that remained constant throughout the deposition.

To interpret the observed capacitance behavior, we propose a model based  
on a simulation of the evolution of the capacitance during the random filling of a  
rectangular mesh grid that represents the area between the IDE digits with NPs,

as illustrated in Figure 1 (d), where grid positions are filled randomly to mimic  
 NP deposition over time. However, considering the aspect ratio between the NP  
 mean diameter and the IDE geometry, it would require dividing the rectangle  
 into a mesh of  $(1.33 \times 10^4) \times (1.0 \times 10^6)$  squares, implying a prohibitive com-  
 putational cost. To overcome this limitation, we propose to analyze a fraction  
 of the IDE, which can further be scaled up to describe the whole system. To  
 support this approach, we recall the interpretation in which filling with nanopar-  
 ticles the space between adjacent digits is equivalent to divide the mesh into  $q$   
 lines and  $q$  rows, maintaining the aspect ratio between the digits space  $s$  and  
 its length  $l$ , i.e.,  $l = 75s$ . These capacitors are coupled in series and in parallel,  
 as sketched in the Figure 5 (a). Assuming that each capacitor has a capacitance  
 $C^*$ , the equivalent capacitance of the  $q$  capacitors in series in each line provides  
 $\frac{1}{C_S} \sum_{i=1}^q \frac{1}{C^*}$  and  $C_S = \frac{C^*}{q}$ . Then the parallel coupling of the  $n$   $C_S$  capacitors  
 provides  $C_{TOTAL} = C_P = \sum_{i=1}^q C_S = \frac{q}{q} C^* = C^*$ . Therefore if we maintain the  
 aspect ratio, the capacitance calculated for a smaller region can be scaled to  
 describe the whole device. Thus, we maintain the nanoparticle size with a lower  
 computational cost. Consequently, we consider a fraction of the whole region,  
 where the spacing  $S$  and length  $L$  is divided in squares of side  $\Delta S = \frac{S}{n}$  and  
 $\Delta L = \frac{L}{m}$ , respectively. To keep the device aspect ratio of the region between  
 digits, we use  $m = 75n$ . Each cell is addressed with a pair of indices,  $(i, j)$ ,  
 with  $i \in [1, n]$  and  $j \in [1, m]$  for the spacing ( $S$ ) and length ( $L$ ) positions, re-  
 spectively. Each column  $j$  is associated with a capacitor  $C_j$  of parallel plates,  
 as depicted in Figure 5 (b). The gap between digits corresponds to the dis-  
 tance between the plates of each  $C_j$  capacitor. The capacitance of this device is  
 thus equivalent to an array of parallel capacitors  $C_j$ , i.e.,  $C(A) = \sum_{j=1}^m C_j(A)$ .  
 Therefore,  $C(A = 0\%) = C_0$ , is the initial value of this capacitance in vacuum,  
 before any deposition. Let a particle be introduced at row  $i$  and column  $j$  in the  
 grid. When  $i$  is the first or last available space in column  $j$  ( $i = 1$  or  $i = n$ ), the  
 capacitance  $C_j$  changes as if the capacitor's gap was reduced by one grid space  
 $\Delta S$ . If instead the particle is introduced at an intermediate space  $1 < i < n$ ,  
 the resulting capacitance  $C_j$  of this channel can be written as two capacitors of

220 reduced gaps operating in series with gaps  $(i - 1)\Delta S$  and  $(n - i)\Delta S$ . Note that  
the total sum of the gaps is also reduced by one grid space like before, but now  
it created two capacitors. In Figure 5 (b), red squares illustrate sites filled with  
NPs.

We must also take into account that NPs agglomerate and that they also  
225 touch the digits, as illustrated in Figure 5 (b). In these situations, empty sites  
can be shielded from the electric field by sites occupied by NPs. The blue  
squares in Figure 5 (b) illustrate situations in which empty sites are shielded by  
agglomerations of NPs, with or without contact with the digits. In the model  
proposed for  $C(A)$ , groups of adjacent particles with at least one connection  
230 to a digit will shield all empty sites between any constituent particles and the  
nearest wall. Shielded sites contribute to  $C(A)$  as if they were occupied.

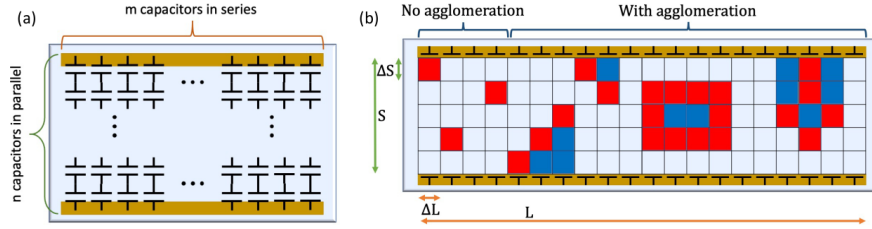


Figure 5: (a) Scheme in which we divided the gap between adjacent digits of the IDE in  $q$  capacitors coupled in series, and  $q$  capacitors coupled in parallel to support the argument that analyzing a small region of the IDE allows scaling the result to describe the whole system. (b) Schematic of the rectangular mesh depicting regions with (right-hand side) and without (left-hand side) agglomeration of NPs. Light blue squares are empty sites; red squares are filled with NPs and dark blue squares are the shielded positions. The simulations discussed in the text were performed for larger meshes ( $S = \Delta S n$  with  $n = 100$ ).

In our experiment, it is not possible to separate  $C(A)$  from the constant capacitance value,  $C'_0$ . As  $C(A)$  is proportional to the initial value  $C(A = 0\%) = C_0$ , we can rewrite it as  $C(A) = k(A)C_0$ . So, we adjusted the proposed model  
235 for  $C(A)$  to the experimental curve considering that  $C_{exp}(A) = k(A)C_0 + C'_0$  and find the values for  $C_0$  and  $C'_0$  to evaluate the total capacitance as a function of  $k(A)$  using our proposed model.

## 5. Discussion

To interpret the conductance behavior in Figure 2, we considered the percolation power-law  $G = G_0(p - p_c)^t$ , in which  $G$  is the experimental conductance,  $G_0$  is a proportionality constant,  $p$  is the percentage of covered area,  $p_c$  is the percolation threshold, and  $t$  is the transport exponent [40]. The optimized fit provided  $p_c = 9\%$  and  $t = 3.939 \pm 0.003$ , as shown in Figure S1. Nevertheless, this  $t$  value is not in accordance with the universal transport exponent that predicts  $t \cong 1.3$ , and  $t \cong 2$ , for two-dimensional, and three-dimensional systems, respectively [41].  $t \approx 3 - 4$  corresponds to tunneling-percolation systems [42], which was evidenced by DC electrical resistivity of co-sputtered Ag-SiO<sub>2</sub> for different metal-insulator ratio [43, 44]. Besides, I. Balberg *et al.* proposed an equation that correlate the non-universal and the universal value of  $t$  to estimate the tunneling range/decay  $d$  [42]. To apply their model, we used the mean nanoparticle radius obtained by TOF (3 nm), and the percolation threshold defined above. The tunneling range  $d \cong 2.5$  nm is accordance with the predictions in the literature [42].

Considering the capacitive component of the impedance, in the previous section, we have proposed a model to calculate the evolution of the capacitance as a function of the covered area. For the calculations, we used a mesh with  $n = 100$ . Figure 6(a) shows the experimental data, the capacitance simulated without considering the agglomeration of NPs, the simulated considering shielded regions due to agglomerated NPs, and the linearly adjusted region used to normalize both simulations to the experimental data. Figure 6(b) presents the number of agglomerations and effective coverage as a function of the covered area. The former is for the number of isolated NPs and the number of groups of NPs that are considered agglomerations in our models. After filling a position in the matrix to be filled, our method analyzes the whole matrix and counts the number of agglomerations in each iteration. The number of agglomerations increases until reaching approximately 20% coverage. Beyond 20% coverage, additional NPs fall on or connect to pre-formed agglomerations, eventually linking

them into bigger agglomerates. The number of agglomerations thus decreases, leading to the bell-like dependence of the number of agglomerations as a function of the covered area seeing in Figure 6(b). The effective coverage refers to the sum of sites in the grid that contain an NP and that shielded by an agglomeration.

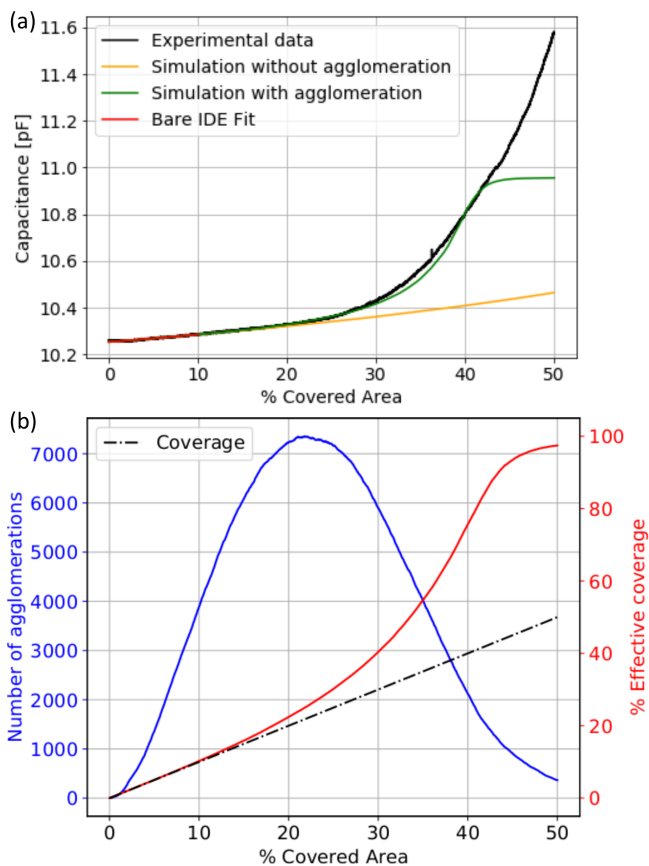


Figure 6: (a) Experimental and simulated values of IDE capacitance during NPs deposition. (b) Left: the sum of the number of isolated NPs and the number of agglomerated NPs; right: % of occupied and shielded positions on the grid. The dashed line describes the % covered area, also associated with right-hand axis.

We see in Figure 6(a) that experimental and simulated results are in good agreement when the linear portion of the curve is considered (up to 20% of coverage). It is important to remark that the model without agglomeration is, in fact, a linear capacitance function of the covered area up to 50% coverage,

and therefore, it is incapable of describing the non-linear behavior observed for coverages higher than  $\sim 20\%$ . Moreover, Figure 6(b) showed that the number of isolated and agglomerated NPs grows until  $\sim 20\%$  of coverage and then goes down. Also, the % effective coverage was linear until  $\sim 20\%$  of the covered area and started to increase rapidly. This behavior indicates that initially, the IDE's capacitance can be described by the effects of isolated NPs.

From 20% coverage onwards, the capacitance begins to be dominated by the existence of agglomeration of NPs that shield regions of the IDE. This can be verified in Figure 6(a), where the simulation with shielded sites due to agglomerated NPs (green curve) follows the experimental data up to  $\sim 45\%$  coverage. Besides, from  $\sim 20\%$  coverage on, the number of agglomerations decreases, indicating that isolated NPs as well as agglomerations start to touch, meaning they coalesce. Also from this point on, the % of effective coverage is no longer linear with the % of the covered area, but grows faster. This result indicates that the contribution of shielded areas, due to NP agglomeration, must be considered in order to understand the IDE capacitance behavior from 20% coverage.

Above 45% coverage, the IDE capacitance in our model saturates, not correctly representing the experimental data. This can be related to the percolation threshold, which adds a resistive component to the device. According to the literature, the percolation occurs for 40% coverage in a square matrix with next-nearest neighbour conductance, from this point on our model is no longer adequate [45]. Besides, the % of effective coverage (occupied and shielded positions on the grid) also saturates. We recall the literature showing a measurable conductive component in electrical transport for over 45% coverage [46], which must contribute to the measurement of our IDE electrical behavior.

We furthermore note here that our simple model correctly reproduces not only the overall trend but can even quantitatively describe the variations in capacitance despite its simplifications. From the AFM image in Figure 3 we can deduce that three-dimensional growth is non-negligible; we have, however, tested that permitting a second layer of deposited NPs in the model has only minor effects. This is comprehensible as additional layers only slightly re-scale

the abscissa of Fig. 6.

## 6. Conclusions

Surface deposition of metal NPs for numerous studies, on the one hand, re-  
310 lies on controlling the low concentration of NP on the substrate. On the other  
hand, works on the electrical properties of films of NPs usually investigate films  
that are close to or above the percolation limit, where electric transport is pre-  
dominately resistive. We have focused in our study on the evolution of the  
sample complex impedance from the very beginning of the NP deposition up to  
315 the percolation limit. The observed variation in capacitance can be divided into  
two regimes, a linear one between 0% and  $\sim 20\%$  coverage, and a non-linear one  
for values above  $\sim 20\%$ . To interpret these results, we propose a simple model  
based on the occupation of sites between digits. The model takes into account  
how agglomeration of NPs leads to the formation of shielded sites that affect the  
320 electric field between electrodes and the capacitance consequently. This model  
shows that the first capacitance regime is dominated by isolated and agglomer-  
ated NPs. Above  $\sim 20\%$  coverage, the capacitance starts having contributions of  
shielded regions between the electrodes due to agglomerated NP islands, lead-  
ing to a super-linear capacitance increase. TEM and AFM micrographs support  
325 our interpretations. The proposed model and electrical behavior analysis open  
possibilities to control the concentration of NP deposited on surfaces for optical,  
magnetic, and catalytic studies. Besides, our work contributes to the develop-  
ment and miniaturization of electronic devices and flexible electronics based on  
IDEs with NPs film. It can also be extended to the deposition of wet-chemically  
330 synthesized NPs, facilitating the comprehension of several phenomena and ef-  
fects caused by NP introduction in a variety of applications in several knowledge  
areas.

## Acknowledgements

The authors are grateful to FAPESP (FAPESP, 2014/03691-7, 2013/14262-7,  
335 2016/12807-4), CNPq, and CAPES for financial support. Experimental support  
from the Microfabrication Laboratory (proposal LMF-18748 and LMF-21855)  
and Electron Microscopy Laboratory (proposal TEM-21702, ME-22308, TEM-  
23432, TEM-24315, TEM-C1-25093) at Brazilian Nanotechnology National Lab-  
oratory (LNNano), CNPEM, Campinas, Brazil for their support with the use  
340 of equipments.

## References

- [1] R. A. Maniyara, D. Rodrigo, R. Yu, J. Canet-Ferrer, D. S. Ghosh, R. Yongsunthon, D. E. Baker, A. Rezikyan, F. J. García de Abajo, V. Pruneri, Tunable plasmons in ultrathin metal films, *Nature Photonics* 13 (5) (2019) 328–333. doi:10.1038/s41566-019-0366-x.  
345 URL <https://doi.org/10.1038/s41566-019-0366-x>
- [2] J. N. Anker, W. P. Hall, O. Lyandres, N. C. Shah, J. Zhao, R. P. Van Duyne, Biosensing with plasmonic nanosensors, *Nanoscience and Technology: A Collection of Reviews from Nature Journals* 7 (June) (2009) 308–319. doi:10.1142/9789814287005\_0032.  
350 URL [https://doi.org/10.1142/9789814287005\\_0032](https://doi.org/10.1142/9789814287005_0032)
- [3] A. Campos, N. Troc, E. Cottancin, M. Pellarin, H.-C. Weissker, J. Lermé, M. Kociak, M. Hillenkamp, Plasmonic quantum size effects in silver nanoparticles are dominated by interfaces and local environments, *Nat. Phys.* 15 (2019) 275–280. doi:10.1038/s41567-018-0345-z.  
355 URL <https://doi.org/10.1038/s41567-018-0345-z>
- [4] H. Wei, H. Eilers, From silver nanoparticles to thin films: Evolution of microstructure and electrical conduction on glass substrates, *Journal of Physics and Chemistry of Solids* 70 (2) (2009) 459–465. doi:<https://doi.org/10.1016/j.jpcs.2008.11.012>.

- 360 URL <http://www.sciencedirect.com/science/article/pii/S0022369708005374>
- [5] L. Liu, A. Corma, Metal Catalysts for Heterogeneous Catalysis: From Single Atoms to Nanoclusters and Nanoparticles, *Chemical Reviews* 118 (10) (2018) 4981–5079. doi:10.1021/acs.chemrev.7b00776.
- 365 URL <https://doi.org/10.1021/acs.chemrev.7b00776>
- [6] C. Bansal, S. G. Praveen, J. T. T. Kumaran, A. Chatterjee, Inter-cluster distance dependence of electrical conduction in nanocluster assembled films of silver: a new paradigm for design of nanostructures, *Scientific reports* 5 (2015) 7685. doi:10.1038/srep07685.
- 370 URL <https://pubmed.ncbi.nlm.nih.gov/25566690><https://www.ncbi.nlm.nih.gov/pmc/articles/PMC4286756/>
- [7] F. Jiménez-Villacorta, C. Munuera, C. Ocal, C. Prieto, Study of nanoconductive and magnetic properties of nanostructured iron films prepared by sputtering at very low temperatures, *Journal of Nanoparticle Research* 12 (4) (2010) 1117–1127. doi:10.1007/s11051-009-9640-z.
- 375 URL <https://doi.org/10.1007/s11051-009-9640-z>
- [8] M. Novotny, J. Bulir, J. Lancok, P. Pokorny, M. Bodnar, In-situ monitoring of the growth of nanostructured aluminum thin film, *Journal of Nanophotonics* 5 (1) (2011) 1–11. doi:10.1117/1.3543816.
- 380 URL <https://doi.org/10.1117/1.3543816>
- [9] N. Abdellaoui, A. Pereira, M. Novotny, J. Bulir, P. Fitl, J. Lancok, B. Moine, A. Pillonnet, In situ monitoring of electrical resistance during deposition of Ag and Al thin films by pulsed laser deposition: Comparative study, *Applied Surface Science* 418 (2017) 517–521. doi:10.1016/j.apsusc.2016.11.234.
- 385 URL <http://dx.doi.org/10.1016/j.apsusc.2016.11.234>
- [10] O. Kylián, J. Prokeš, O. Polonskyi, J. Čechvala, J. Kousal, J. Pešíčka, J. Hanuš, H. Biederman, Deposition and characterization of Pt nanocluster

- films by means of gas aggregation cluster source, *Thin Solid Films* 571 (P1)  
390 (2014) 13–17. doi:10.1016/j.tsf.2014.09.064.
- [11] N. Maréchal, E. Quesnel, Y. Pauleau, Silver thin films deposited  
by magnetron sputtering, *Thin Solid Films* 241 (1) (1994) 34–38.  
doi:[https://doi.org/10.1016/0040-6090\(94\)90391-3](https://doi.org/10.1016/0040-6090(94)90391-3).  
URL [http://www.sciencedirect.com/science/article/pii/](http://www.sciencedirect.com/science/article/pii/S0040609094903913)  
395 [0040609094903913](http://www.sciencedirect.com/science/article/pii/S0040609094903913)
- [12] K. Y. Chan, B. S. Teo, Sputtering power and deposition pressure ef-  
fects on the electrical and structural properties of copper thin films,  
*Journal of Materials Science* 40 (22) (2005) 5971–5981. doi:10.1007/  
s10853-005-1362-8.
- 400 [13] U. B. Arnalds, J. S. Agustsson, A. S. Ingason, A. K. Eriksson, K. B. Gyl-  
fason, J. T. Gudmundsson, S. Olafsson, A magnetron sputtering system  
for the preparation of patterned thin films and in situ thin film electrical  
resistance measurements, *Review of Scientific Instruments* 78 (10) (2007)  
1–6. doi:10.1063/1.2793508.
- 405 [14] E. Barborini, G. Corbelli, G. Bertolini, P. Repetto, M. Leccardi, S. Vinati,  
P. Milani, The influence of nanoscale morphology on the resistivity of  
cluster-assembled nanostructured metallic thin films, *New Journal of  
Physics* 12 (7) (2010) 73001. doi:10.1088/1367-2630/12/7/073001.  
URL <https://doi.org/10.1088/1367-2630/12/7/073001>
- 410 [15] A. Sattar, S. Fostner, S. A. Brown, Quantized conductance and switching  
in percolating nanoparticle films., *Phys. Rev. Lett.* 111 (2013) 136808. doi:  
10.1103/PhysRevLett.111.136808.
- [16] C. Minnai, A. Bellacicca, S. A. Brown, P. Milani, Facile fabrication of  
complex networks of memristive devices, *Scientific Reports* 7 (1) (2017)  
415 1–8. doi:10.1038/s41598-017-08244-y.

- [17] M. Mirigliano, F. Borghi, A. Podestà, A. Antidormi, L. Colombo, P. Milani, Non-ohmic behavior and resistive switching of Au cluster-assembled films beyond the percolation threshold, *Nanoscale Advances* 1 (8) (2019) 3119–3130. doi:10.1039/c9na00256a.
- 420 [18] A. Vahl, N. Carstens, T. Strunskus, F. Faupel, A. Hassanien, Diffusive Memristive Switching on the Nanoscale, from Individual Nanoparticles towards Scalable Nanocomposite Devices, *Scientific Reports* 9 (1) (2019) 1–10. doi:10.1038/s41598-019-53720-2.  
URL <http://dx.doi.org/10.1038/s41598-019-53720-2>
- 425 [19] J. Schmelzer, S. A. Brown, A. Wurl, M. Hyslop, R. J. Blaikie, Finite-size effects in the conductivity of cluster assembled nanostructures, *Phys. Rev. Lett.* 88 (2002) 226802. doi:10.1103/PhysRevLett.88.226802.  
URL <https://link.aps.org/doi/10.1103/PhysRevLett.88.226802>
- [20] V. Popok, Ion implantation of polymers: Formation of nanoparticulate materials, *Reviews on Advanced Materials Science* 30 (2012) 1–26.
- 430 [21] M. C. Salvadori, M. Cattani, F. S. Teixeira, I. G. Brown, Conducting polymer formed by low energy gold ion implantation, *Applied Physics Letters* 93 (7) (2008) 73102. doi:10.1063/1.2973161.  
URL <https://doi.org/10.1063/1.2973161>
- 435 [22] C. Binns (Ed.), *Nanomagnetism: Fundamentals and Applications*, Volume 6, 1st Edition, Elsevier, Amsterdam, Netherlands, 2014.
- [23] S. Oyarzún, A. Tamion, F. Tournus, V. Dupuis, M. Hillenkamp, Size effects in the magnetic anisotropy of embedded cobalt nanoparticles: From shape to surface, *Scientific Reports* 5 (August) (2015) 16–21. doi:10.1038/srep14749.
- 440 [24] U. Heiz, U. Landman (Eds.), *Nanocatalysis*, Springer Berlin Heidelberg,

2007. doi:10.1007/978-3-540-32646-5.

URL <https://doi.org/10.1007%2F978-3-540-32646-5>

445 [25] P. Anger, P. Bharadwaj, L. Novotny, Enhancement and Quenching of  
Single-Molecule Fluorescence, *Physical Review Letters* 96 (11) (2006)  
113002. doi:10.1103/PhysRevLett.96.113002.

URL <https://link.aps.org/doi/10.1103/PhysRevLett.96.113002>

[26] E. Cottancin, G. Celep, J. Lermé, M. Pellarin, J. R. Huntzinger, J. L. Vialle,  
450 M. Broyer, Optical Properties of Noble Metal Clusters as a Function of  
the Size: Comparison between Experiments and a Semi-Quantal Theory,  
*Theoretical Chemistry Accounts* 116 (4) (2006) 514–523. doi:10.1007/  
s00214-006-0089-1.

URL <https://doi.org/10.1007/s00214-006-0089-1>

455 [27] A. R. Guerrero, R. F. Aroca, Surface-Enhanced Fluorescence with  
Shell-Isolated Nanoparticles (SHINEF), *Angewandte Chemie International  
Edition* 50 (3) (2011) 665–668. doi:10.1002/anie.201004806.

URL [https://onlinelibrary.wiley.com/doi/abs/10.1002/anie.  
201004806](https://onlinelibrary.wiley.com/doi/abs/10.1002/anie.201004806)

460 [28] R. C. Hensel, M. Moreira, A. Riul Jr, O. N. Oliveira Jr, V. Rodrigues,  
M. Hillenkamp, Monitoring the dispersion and agglomeration of silver  
nanoparticles in polymer thin films using localized surface plasmons and  
ferrell plasmons, *Appl. Phys. Lett.* 116 (10) (2020) 103105.

URL <https://doi.org/10.1063/1.5140247>

465 [29] J. Ferreira, F. S. Teixeira, A. R. Zanatta, M. C. Salvadori, R. Gor-  
don, O. N. Oliveira, Tailored SERS substrates obtained with cathodic  
arc plasma ion implantation of gold nanoparticles into a polymer ma-  
trix, *Physical Chemistry Chemical Physics* 14 (6) (2012) 2050–2055. doi:  
10.1039/C2CP23287A.

470 URL <http://dx.doi.org/10.1039/C2CP23287A>

- [30] D. Keith Roper, K. R. Berry, A. G. Russell, P. A. Blake, D. Keith Roper, Gold nanoparticles reduced in situ and dispersed in polymer thin films: Optical and thermal properties, *Nanotechnology* 23 (37) (2012). doi:10.1088/0957-4484/23/37/375703.
- 475 [31] O. N. Oliveira, R. M. Iost, J. R. Siqueira, F. N. Crespilho, L. Caseli, Nanomaterials for Diagnosis: Challenges and Applications in Smart Devices Based on Molecular Recognition, *ACS Applied Materials & Interfaces* 6 (17) (2014) 14745–14766. doi:10.1021/am5015056.  
URL <https://doi.org/10.1021/am5015056>
- 480 [32] L. A. Mercante, V. P. Scagion, A. Pavinatto, R. C. Sanfelice, L. H. C. Mattoso, D. S. Correa, Electronic Tongue Based on Nanostructured Hybrid Films of Gold Nanoparticles and Phthalocyanines for Milk Analysis, *Journal of Nanomaterials* 2015 (2015) 890637. doi:10.1155/2015/890637.  
URL <https://doi.org/10.1155/2015/890637>
- 485 [33] S. Choudhury, R. Mangal, A. Agrawal, L. A. Archer, A highly reversible room-temperature lithium metal battery based on crosslinked hairy nanoparticles, *Nature Communications* 6 (1) (2015) 10101. doi:10.1038/ncomms10101.  
URL <https://doi.org/10.1038/ncomms10101>
- 490 [34] A. D. T. de Sá, V. T. Abrao Oiko, G. di Domenicantonio, V. Rodrigues, New experimental setup for metallic clusters production based on hollow cylindrical magnetron sputtering, *Journal of Vacuum Science & Technology B, Nanotechnology and Microelectronics: Materials, Processing, Measurement, and Phenomena* 32 (6) (2014) 061804. doi:10.1116/1.4900847.  
495 URL <http://avs.scitation.org/doi/10.1116/1.4900847>
- [35] H. Haberland, M. Karrais, M. Mall, Y. Thurner, Thin films from energetic cluster impact: A feasibility study, *Journal of Vacuum Science & Technology A: Vacuum, Surfaces, and Films* 10 (5) (1992) 3266–3271. doi:10.1116/1.577853.

- 500 [36] M. Hillenkamp, G. Di Domenicantonio, O. Eugster, C. Félix, Instability of Ag nanoparticles in SiO<sub>2</sub> at ambient conditions, *Nanotechnology* 18 (2007) 015702. doi:10.1088/0957-4484/18/1/015702.  
URL <https://doi.org/10.1088/0957-4484/18/1/015702>
- [37] R. C. Hensel, K. L. Rodrigues, V. D. L. Pimentel, A. Riul, V. Rodrigues,  
505 Automated self-assembly and electrical characterization of nanostructured films, *MRS Communications* 8 (2) (2018) 283–288. doi:10.1557/mrc.2018.47.
- [38] M. W. Den Otter, Approximate expressions for the capacitance and electrostatic potential of interdigitated electrode, *Sensors and Actuators, A: Physical* 96 (2-3) (2002) 140–144. doi:10.1016/S0924-4247(01)00783-X.  
510
- [39] R. Igreja, C. J. Dias, Analytical evaluation of the interdigital electrodes capacitance for a multi-layered structure, *Sensors and Actuators A: Physical* 112 (2) (2004) 291–301. doi:<https://doi.org/10.1016/j.sna.2004.01.040>.  
515 URL <http://www.sciencedirect.com/science/article/pii/S0924424704000779>
- [40] N. Johner, C. Grimaldi, I. Balberg, P. Ryser, Transport exponent in a three-dimensional continuum tunneling-percolation model, *Physical Review B* 77 (17) (2008) 174204. doi:10.1103/PhysRevB.77.174204.  
520 URL <https://link.aps.org/doi/10.1103/PhysRevB.77.174204>
- [41] C. Grimaldi, Theory of percolation and tunneling regimes in nanogranular metal films, *Physical Review B* 89 (21) (2014) 214201. doi:10.1103/PhysRevB.89.214201.  
URL <https://link.aps.org/doi/10.1103/PhysRevB.89.214201>
- 525 [42] I. BALBERG, D. AZULAY, D. TOKER, O. MILLO, PERCOLATION AND TUNNELING IN COMPOSITE MATERIALS, *International Journal of Modern Physics B* 18 (15) (2004) 2091–2121. doi:10.1142/

S0217979204025336.

URL <https://doi.org/10.1142/S0217979204025336>

- 530 [43] E. B. Priestley, B. Abeles, R. W. Cohen, Surface plasmons in granular Ag-SiO<sub>2</sub> films, Physical Review B 12 (6) (1975) 2121–2124. doi:10.1103/PhysRevB.12.2121.

URL <https://link.aps.org/doi/10.1103/PhysRevB.12.2121>

- [44] B. ABELES, Granular Metal Films, in: R. B. T. A. S. S. S. Wolfe (Ed.), Applied Solid State Science, Vol. 6, Elsevier, 1976, pp. 1–117. 535 doi:<https://doi.org/10.1016/B978-0-12-002906-8.50007-X>.

URL <http://www.sciencedirect.com/science/article/pii/B978012002906850007X>

- [45] P. Grassberger, Conductivity exponent and backbone dimension in 2-d 540 percolation, Physica A: Statistical Mechanics and its Applications 262 (3) (1999) 251–263. doi:[https://doi.org/10.1016/S0378-4371\(98\)00435-X](https://doi.org/10.1016/S0378-4371(98)00435-X).

URL <http://www.sciencedirect.com/science/article/pii/S037843719800435X>

- 545 [46] A. K. Ahmad, B. L. Evans, A resistance network representation of electrical conduction in Pt and Cu films, Surface Science 364 (1) (1996) 39–53. doi:[https://doi.org/10.1016/0039-6028\(96\)00589-4](https://doi.org/10.1016/0039-6028(96)00589-4).

URL <http://www.sciencedirect.com/science/article/pii/0039602896005894>